CHAPTER IV
CHITOSAN NANOSCAFFOLD INJECTABLE GEL: A UNIQUE BONE GLUE BIONANOCOMPOSITES

4.1 Abstract

Injectable bone glue is a potential material for bone healing due to the possibility of direct injection into bone breaking area, the efficient bone connection through chemical and/ or physical bonds, and the convenient clinical treatment without surgery. Chitosan is a good candidate since it is not only glucosamine via enzymatic degradation, a major component of bone marrow, but also it can be derivatized to highly viscous or gel-type glue. Herein, we propose a novel bone glue bionanocomposite based on chitosan nanoscaffold, CN. The advantages of using CN are the ease of derivatization to be water soluble species (carboxymethylchitosan nanoscaffold, CMCN), the effective heterogeneous reaction to obtain epoxidized CN, and the possibility to use as reinforce material in gel network. The CN gel shows biocompatibility as shown from the SaOs-2 cell culture test. The CN also help the gel incorporation with hydroxyapatite as evidenced from optical microscope and scanning electron microscope (SEM).

Keyword: Chitosan nanoscaffold, Injectable gel, Carboxymethylchitosan, Bone glue

4.2 Introduction

Bone is an important rigid organ of human body to sustain and protect internal organs as well as to support the muscle movement. Bone related problems, such as breaking, fracturing, cracking, etc. are still in the needs of the curing process with effectiveness, efficiency, and convenience. The ways to treat the bone fractures are depending on the position of breakage and/or the level of severity. Traditional bone therapy techniques, such as: splints, plaster cast, and metal implantation are usually applied to maintain the bones and allow new bone tissue to regenerate. However, these techniques require the long curing time (3-6 months) depending on patient conditions. In order to minimize the healing time and to prevent the dwarf muscle from inactiveness while maximize the efficiency of bone immobilization, tissue engineering such as ultrasound [1], magnetic [2], autograft [3], and allograft [4] were proposed. However, some limitations have to be admitted. For example, the ultrasound and magnetic techniques need the specific system and equipment set up, the autograft is depending on the existence of donor and morbidity of donor site whereas the allograft has to be aware of immune response risks. Therefore, bone healing technique based on the patient self healing with the helps from functional biomaterials to enhance the bone growth is an ideal case.

Recently, three-dimensional (3D) scaffold for bone regeneration has received much attention. Porous polymers with high mechanical properties as well as bio-related properties, especially bone cell compatibility were reported [5], [6], [7]. Chitosan is a good candidate due to its biocompatibility, biodegradability, bioactivity, and nontoxicity [8], [9], [10]. The fact that the structure of chitosan consists of glucosamine unit, this brings an expectation for the role of lubricant in human joint [11], [12]. On the viewpoint of tissue engineering, chitosan is also a good choice for being biological primer for cell-tissue proliferation and reconstruction including providing the matrices for bone regeneration [13], [14]. For the past few years, our group succeeded in preparing chitosan nanoscaffold, CN, from chitin whisker, CW, [15], [16]. The morphology is under three dimensional nano-fiber networks with high surface area and pore volume (Fig. 4.1).

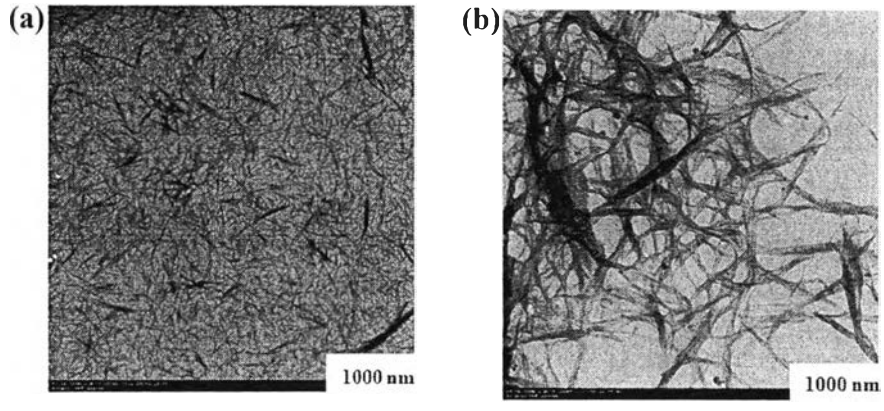

Fig. 4.1 TEM micrographs of (a) CW, and (b) CN.

To our idea, bone glue under the combination of injectable gel and 3D porous scaffold, in other words, bionanocomposite should be an ideal material. At the first step, the material can be directly injected into the specific position of the rapture bone and consequently the gelation allows the bone connection through the covalent and non-covalent bonds. An addition of 3D porous chitosan nanoscaffold makes the bionanocomposite gel obtained enhance bone regeneration. Based on this concept, we propose carboxymethylchitosan, CMC, [17], [18], [19] as water soluble chitosan which produces from CN to obtain carboxymethylchitosan nanoscaffold, CMCN as fluid gel matrices. The advantage of CMCN is also related to the solubility in water to avoid the use of any organic solvents.

Here, three types of gels are in our consideration. The first type is the gelation of CMCN in water when crosslinker, such as epichlorohydrin, was added to obtain CMCN gel. The CMCN gel can be reinforced with CN nano-fibers by simply blending CMCN with CN and adding epichlorohydrin to obtain CMCNB bionanocomposite gel.

The chemical modification of CN with epoxy group to obtain epoxy-chitosan nanoscaffold (ECN), and mixing the ECN with CMCN in water, leads us to another type of bionanocomposite gel, i.e. CMCNE gel, can be achieved. This gel is a bionanocomposite between chitosan network and ECN nano-fibers. The

fact that the crosslink of epoxy group might also form with ECN nano-fibers, the gel with good miscibility and toughness can be expected.

The work also extends to the studies on cell viability including the studies on gel strength and bone cell growth to evaluate the functions of CN and ECN on the three types of the gels.

4.3 Experimental

4.3.1 Materials

Chitin from shrimp shells was provided by Seafresh (Lab) Company Limited, Thailand. Sodium hydroxide, hydrochloric acid, methanol, and isopropanol were purchased from RCI Labscan Limited, Thailand. Epichlorohydrin (C_3H_5ClO) and chloroacetic acid ($ClCH_2COOH$) were purchased from Sigma–Aldrich. All chemicals were used as received without further purification.

4.3.2 Instrument and Equipment

Fourier Transform Infrared Spectrophotometer (FTIR)

Structural characterization related to functional groups was done by a Nicolet/Nexus 670 with 32 scan at a resolution of 4 cm^{-1}, and recorded in frequency range of 4000-650 cm^{-1}.

Nuclear Magnetic Resonance Spectrometer (NMR)

Structural characterization related to types of protons was done by a Bruker Avance proton-nuclear magnetic resonance spectrometer (^1H NMR) 500MHz, and recorded chemical shift from 16 to 0 ppm.

Thermal Gravimetric Analysis (TGA)

Thermal stability of the chitosan gel was determined by a Dupont thermo gravimetric analyzer under N_2 atmosphere at the temperature range between 50°C to 800°C and heating rate of 10°C/min.

Scanning Electron Microscope (SEM)

Morphology of the injectable gel was studied by a Hitachi scanning electron microscope (SEM). The gel samples were cut and coated with a platinum thin layer.

Transmission Electron Microscope (TEM)

Morphology of nanofiber was studied by using a Hitachi transmission electron microscope (TEM). The samples were dispersed in water and dropped on copper grids.

Rheometry

The rheological measurements were performed by using a Rheometric Scientific (TA Instruments). The samples were placed between parallel plate geometry and dropped with mineral oil in order to prevent evaporation during the measurements. The dynamic strain sweep test was applied to determine storage modulus (G′) and loss modulus (G″).

4.3.3 Preparation of Chitosan Nanoscaffold

Chitin whiskers, CW, were prepared as described by Nair and Dufresne [20] with some modifications. In brief, chitin, (1.00 g), was treated in 3 M HCl (100.0 ml) and stirred at 105 °C for 3 h to obtain colloidal solution. The solution was centrifuged, followed by treating with hydrochloric acid for two times and dialyzing in distilled water, before lyophilizing to obtain white fine fibrous product of CW (Scheme 4.1).

FTIR (KBr, cm^{-1}): 3485, 3310 and 3120 (-OH and -NH) 1663, 1627, and 1560 (amides I and II).

Chitosan nanoscaffold, CN, was prepared as previously described by Phongying et al. In brief, CW (20 ml, 2.45 g) was stirred in aq. NaOH (40% w/v, 100.0 ml) at 150 °C for 7 h and left at room temperature overnight. The precipitates were collected followed by treating for two more times with NaOH to accomplish the treatment time of 21 h. The crude product was dialyzed in distilled water several times until neutral, and lyophilized to obtain white fine fiber of CN (Scheme 4.1).

FTIR (KBr, cm^{-1}): 3484 (-OH), 1640 (amide I), 1595 ($-NH_2$), and 1154-896 (pyranose ring). ^{1}H-NMR (δ, ppm, 500 Hz, 2% CD_3COOD/D_2O, 338 K): 2.472 (NHAc), 3.593 (H2 of GlcN unit in chitosan), 4.412-4.305 (H2 of GlcNAc and H3-H6 of pyranose ring), 4.927 (H1 of GlcNAc), 5.274 (H1 of GlcN).

3 M HCl
3 times

12 M NaOH
3 times

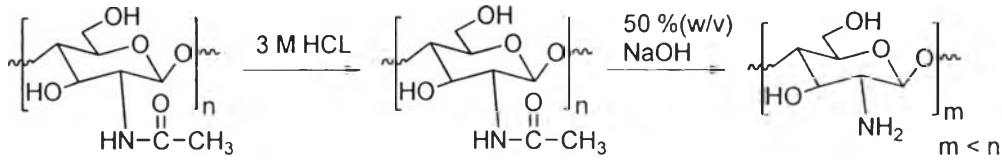

Chitin | Chitin Whisker CW | Chitosan Nanoscaffold CN

Scheme 4.1 Preparation of chitin whisker and chitosan nanoscaffold

Molecular weight (Mw) of CN was determined based on pullulan standards by using a Shimadzu LC-10AD, size exclusion chromatography (SEC) equipped with a TSK-GEL WS44228 column (7.8 mm × 300 mm; Milford; Massachusetts, USA) under the conditions of an eluent flow rate at 1.0 ml/min operating temperature at 40 °C, and, [21]. The eluent was 0.5 mol/L CH_3COOH/ 0.5 mol/L CH_3COONa aqueous solution. Pullulans were products of Showa Denso K.K. with Mw of 6.0×10^3, 1.0×10^4, 2.2×10^4, 4.9×10^4, 1.1×10^5, and 2.1×10^5, 3.9×10^5, 8.1×10^5, as evaluated by using 0.5 mol/L CH_3COOH/ 0.5 mol/L CH_3COONa aqueous solution at 1 mg/mL. Pullulans were filtered through 0.45 mm millipore filters and the weight-average molecular weight was calculated by the following equation.

$$\text{Log (Mw)} = -0.4734\text{Rt} + 12.659 \ (R^2 = 0.9996) \qquad (1)$$

whereas Rt is the retention time.

The Mw of chitosan nanoscaffold is about 103 kDa ± 6.5 kDa and polydispersity (PDI) of CN is 3.0.

4.3.4 Synthesis of Carboxymethylchitosan Nanoscaffold, CMCN

Compound CN (10.0 g/ 6.2 mmol) was suspended in 50% (w/v) NaOH (100 ml) for 1 h at room temperature and kept at -40 °C overnight, then thawed at room temperature. The alkali chitosan was suspended in isopropanol (75 ml), refluxed at 85 °C for 2 h before cooling to room temperature. Chloroacetic acid, $ClCH_2COOH$ 60% (w/v) (100 ml/ 64.8 mmol), was added to the alkali chitosan solution in five equal portions every 5 min before raising to 60 °C and stirring for 4 h. The solution obtained was centrifuged and collected followed by adjusting pH to 7.0 with 1.0 M NaOH. The solution was precipitated in cold methanol and washed with methanol/

H_2O (60: 40) several times. The product was dissolved in water, filtrated out the insoluble particles and freeze-dried at -50 °C to obtain white powder of CMCN (Scheme 4.2). The solubility of CMCN was applied to see the rang of pH and concentration for using CMCN as a liquid phase.

FTIR (KBr, cm^{-1}): 3467 (-OH), 1609 (-COO-), 1418 (-COO-), and 1164-893 (pyranose ring). ^{1}H-NMR (δ, ppm, 500 Hz, D_2O, 298 K): 4.7-5.0 (H1 of GlcN), 4.5-4.7 (H1 of GlcNAc), 4.3-4.4 (H3 of O-CH_2COOH), 4.0-4.3 (H6 and H3 of O-CH_2COOH), 3.3-4.0 (H3-6 of pyranose ring), 3.0-3.3 (H2 of N-CH_2COOH), 2.7-3.0 (H2 of GlcN unit in chitosan), 2.1 (H2 GlcN unit in chitin).

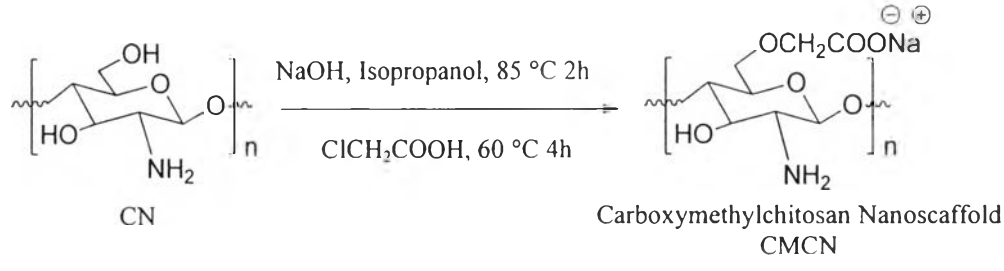

CN

Carboxymethylchitosan Nanoscaffold
CMCN

Scheme 4.2 Synthesis of carboxymethylchitosan nanoscaffold

4.3.5 Synthesis of Epoxy-chitosan Nanoscaffold (ECN)

Compound CN (1.00 g) was suspended in 25% (w/v) NaOH, and NaOH, and epichlorohydrin, EPC (2.0 ml) was added before stirring at 50 °C for 24 h (Scheme 4.3). The heterogeneous solution was filtrated to collect the white precipitates. The precipitates were washed with methanol several times to obtain epoxy-chitosan nanoscaffold (ECN).

FTIR (KBr, cm^{-1}): 3400 (-OH), 2929 (-CH), 1432 (-CH_2), 1150-1085 (-CH_2-O-CH_2), 928 (oxirane ring), and 729 (-CH_2-Cl).

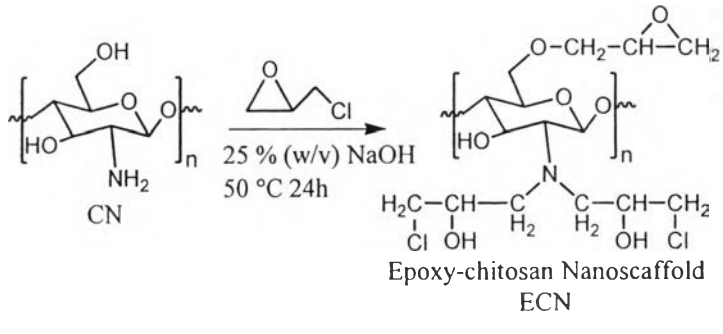

Epoxy-chitosan Nanoscaffold
ECN

Scheme 4.3 Synthesis of epoxy-chitosan nanoscaffold

4.3.6 Preparation of Carboxymethylchitosan Nanoscaffold Gel, CMCN Gel

Compound CMCN, (20 mg), was added in deionized water 1.0 ml to obtain CMCN-2 (2% (w/v)). In similar, CMCN 1or, 40, 60, 80, 100, 150 and 200 mg, also added in deionized water 1.0 ml to obtain CMCN-4, -6, -8, -10, -15, and -20. The pH values of the solutions were in the range of 6.80-7.40. EPC was added for 0.05, 0.1, 0.2, 0.3, 0.4, and 0.5 ml to investigate appropriate amount of crosslink agent. Gelation time and gelation temperature were systematically examined by test tube inverting method. The temperature was varied from room temperature to 60 °C.

FTIR (KBr, cm^{-1}): 3426 (-OH), 1736 (-C=O ester linkage), 1598 ($-NH_2$), and 1151-898 (pyranose ring).

4.3.7 Preparation of Gel by Blending CMCN with CN, CMCNB Gel

CN (20 mg) was blended with the aqueous solution of CMCN-10 (10% (w/v)). The mixture was allowed stirring and sonicating for 15 min. EPC (0.2 ml) was added into the mixture and allowed stirring and sonicating until the solution obtained became a fluid viscous gel. The fluid gel was transferred to syringe before gelation of CMCNB-2 gel was completed. The fluid gel was injected into the mold to determine percent swelling of CMCNB-2 gel. In similar, a series of CN contents, i.e. 50, 100, 200, 400, and 600 mg, were added into solutions of CMCN-10 to form CMCNB-5, -10, -20, -40, and -60 gels.

FTIR (KBr, cm^{-1}): 3426 (-OH), 1737 (-C=O ester linkage), 1597 ($-NH_2$ high intensity), and 1150-898 (pyranose ring).

4.3.8 Preparation of Gel by Crosslinking between CMCN and ECN, CMCNE Gel

ECN, (20 mg), was added in the solution of CMCN-10 (10% (w/v)). The mixture were allowed stirring and sonicating for 15 min. EPC (0.2 ml) was added into the mixture and allowed stirring and sonicating until the solution obtained became a fluid viscous gel. The fluid gel was transferred to syringe before gelation of CMCNE-2 was completed. The fluid gel was injected into the mold to determine percent swelling of CMCNE gel. In similar, a series of ECN contents, i.e. 50, 100, 200, 400,

and 600 mg, were added into solution of CMCN-10 to form CMCNE-5, -10, -20, -40, and -60 gels.

FTIR (KBr, cm^{-1}): 3426 (-OH), 1736 (-C=O ester linkage), 1596 ($-NH_2$), and 1151-898 (pyranose ring).

4.3.9 Swelling Measurement

Gel was cut into pieces with the size of 1.0 × 1.0 × 0.3 cm and was weighed (m_b) before placing in distilled water at room temperature. The gel was taken out of water at regular time, and then the water on the gel was removed thoroughly by filter paper. The gel after time t immersing in water was weighed, m_t. The gel was weighed until constant (m_e). The gel was weighed at dry state (m_0). The percentage of

$$\% \text{ Swelling} = \frac{(m_t - m_b)}{m_b} \times 100 \qquad (2)$$

$$EWC = \frac{(m_e - m_0)}{m_0} \qquad (2)$$

swelling, %S, and equilibrium water content, EWC, were calculated as equations (2) and (3), respectively [22].

The kinetic data of swelling process were used to study water diffusion into gels via equations (4) [23], [24].

$$\frac{M_t}{M_\infty} = kt^n \qquad (3) \quad (4)$$

M_t and M_∞ represent the mass of water absorbed by the hydrogel at time t and at equilibrium whereas k is a gel characteristic constant, which is related to the structural characteristics of the polymer, especially the interaction with the solvent. Swelling exponential, n, describes the mechanism of water penetrated into the hydrogel. The constants n and k were calculated from slope and intercept of log M_t/M_∞ versus log t for the hydrogel.

4.3.10 Network Parameters

The number average molecular weight between crosslink, M_c is one of the basic parameters to describe the crosslink polymeric networks. M_c was calculated by

$$M_c = \frac{-d_p V_s \phi^{1/3}}{[\ln(1-\phi) + \phi + \chi\phi^2]}$$

using equilibrium swelling theory [25], [26], as described previously by Flory and Rehner equation, Eq. (5). The volume fraction of polymer, ϕ, in the swollen state explained about the amount of liquid which can be imbibed into a hydrogel and is defined as a ratio of the polymer volume to the swollen gel volume, Eq. (6) [27].

$$\phi = \left(1 + \frac{d_p}{d_s} \left[\frac{m_a}{m_b} \right] - \frac{d_p}{d_s} \right)^{-1} \qquad (6)$$

Herein, ϕ is volume fraction of polymer in hydrogel, V_s is molar volume of solvent (18 cm^3/mol), χ is Flory-Huggins polymer-solvent interaction parameter, d_s and d_p are the density of solvent and polymer, respectively. The terms of m_a and m_b are the mass of polymer after and before swelling. The χ parameters of hydrogels can be examined from experiment by using equation (7) [28].

$$\chi = \frac{1}{2} + \frac{\phi}{3} \qquad (7)$$

As shown in Eq. (7), χ parameter is always ≥ 0.50. The crosslink density, V_e, can be determined by using Eq. (8). Herein, N_A is Avagadro's number (6.023×10^{23} mol^{-1}) [29].

$$V_e = \frac{d_p N_A}{M_c} \qquad (8)$$

4.3.11 Morphology of Injectable Gel

Morphologies of CMCN-10 gel, CMCNB-10 gel, and CMCNE-10 gel were investigated by both optical, and scanning electron microscopes (SEM). In the case of investigation by SEM, CMCN-10 gel, CMCNB-10 gel, and CMCNE-10 gel were lyophilized before placing on aluminum stub with conductive paint and were sputter-coated with platinum.

4.3.12 Rheological Analysis

The rheological measurements were performed by using a Rheometric Scientific (TA Instruments) at 25 °C with parallel plate geometry (plate diameter of

25 mm, gap of 3 mm). In order to determine storage modulus (G′) and loss modulus (G″), CMCN-10 gel, CMCNB-10 gel, and CMCNE-10 gel were placed on parallel plate and were dropped with mineral oil before measurements. The dynamic strain sweep test was applied with percent strain from 0.1 to 100 at a constant frequency (ω = 1 rad/s)[30].

4.3.13 Hydroxyapatite Cooperation [31]

CMCN-10 gel, CMCNB-10 gel, and CMCNE-10 gel, (1.00 g), were soaked in $CaCl_2$ (200 mM)/Tris-HCl (pH 7.4) aqueous solution (20 ml) at 37 °C for 2 h followed by washing several times with deionized water. The products were soaked in Na_2HPO_4 (120 mM) aqueous solution (20 ml) at 37 °C for 2 h and washed thoroughly with water. Five cycles of soaking were operated.

4.3.14 Cell Culture Studies

Cell culture studies were studied by using a non-transformed cell line SaOs-2 cells (sarcoma osteogenic). The SaOs-2 with 90–95% obtained from T-75 flask cultures were used to seed onto CMCN-10 gel, CMCNB-10 gel, and CMCNE-10 gel. All gels were prepared in 24-well culture plate and incubated with culture medium for 3 h at 37 °C in an incubator with 5% CO_2 and 95% air. Cells were dropwisely seeded onto the top of the gels (5×10^4 cells/50 μl of media/gel). The seeded gels were kept at 37 °C in an incubator with 5% CO_2 for 6 h, 1d, 3d, 5d, and 7d to determine the number of cells in gel by DNA assay technique. The fresh media were changed every two days. The number of cells was analyzed by fluorescent bisbenzimide (Hoechst 33258). Fluorescent measurement used to evaluate cell number by converted from calibration curve of known cell number at 355 nm (excitation) and 460 nm (emission) using fluorescent microplate readers.

4.4 Results and Discussion

4.4.1 Structural Characterization

Chemical structures and morphologies of CW and CN were confirmed to be chitin whisker and chitosan nanoscaffold as reported elsewhere and in Fig. 4.1. In addition, the average degree of deacetylation of CN was 93 as evaluated by ^{1}H-NMR. When CN was modified to CMCN (Fig. 4.2(d)), it shows a significant peak of COO^- at 1609 and 1418 cm^{-1}. The heterogeneous reaction of CN with EPC resulted in ECN as identified from a new at 907 cm^{-1} and -CH_2-Cl at 726 cm^{-1} referring to an oxirane ring (Fig. 4.2(c)). By mixing EPC with CMCN, the gelation was easily observed. As shown in Scheme 4.4, the gelation mechanism might progress continuously via nucleophilic reaction between epoxy group and carboxyl groups to obtain viscous solution and become gel at the final stage. The chemical structure of CMCN gel was relevant to the mechanism of which an ester bond at 1737 cm^{-1} as a consequence of the crosslinked reaction with EPC could be identified (Fig. 4.2(e)). The reaction was accomplished at room temperature suggesting that the gelation was possible at below body temperature.

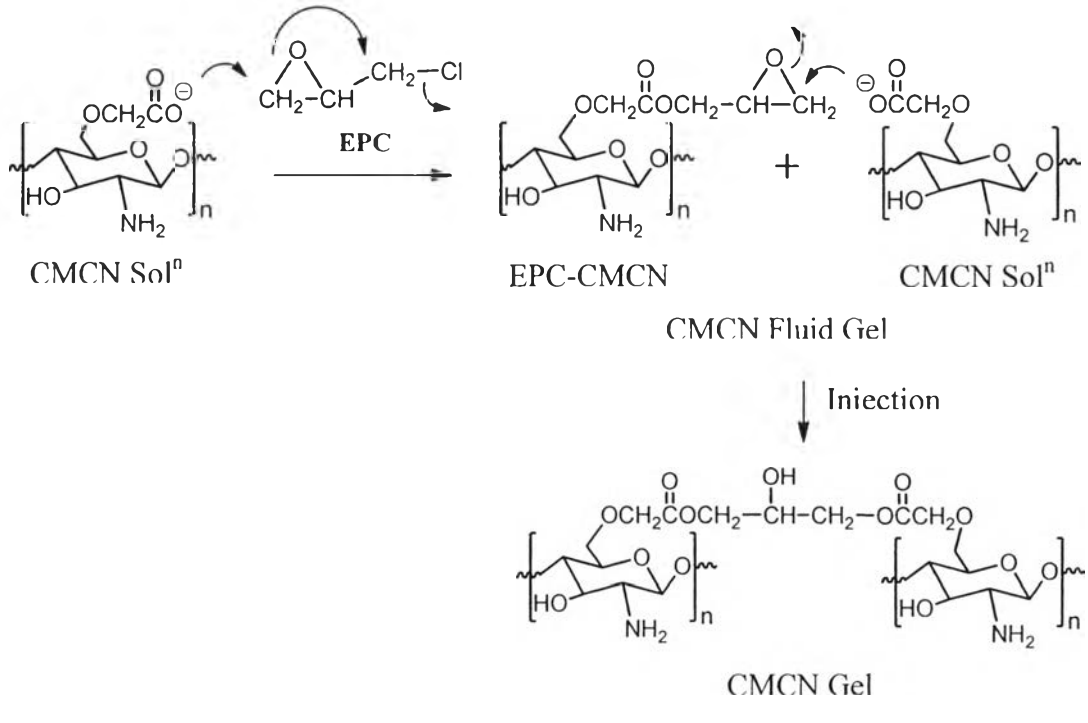

Scheme 4.4 Expected mechanism of CMCN gel

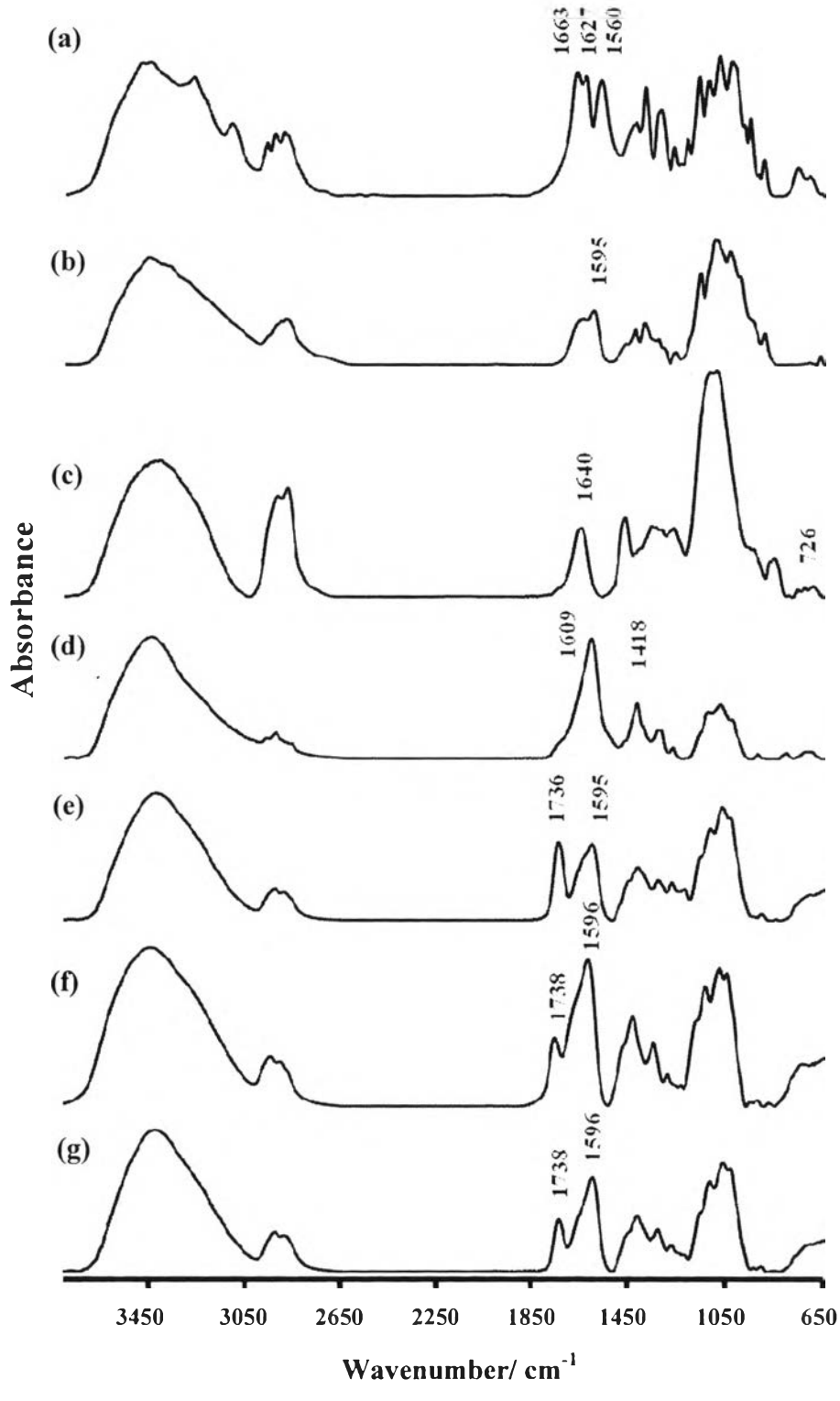

Fig. 4.2 FTIR spectra of (a) CW, (b) CN, (c) ECN, (d) CMCN, (e) CMCN-10 gel, (f) CMCNB-10 gel, and (g) CMCNE-10 gel.

It is important to note that when CN was further added in CMCN solution crosslinked with EPC, a gelation of CMCNB was also observed. Fig. 4.2(f) shows FTIR spectrum of CMCNB gel with a significant increase of the peak at 1598 cm^{-1} indicating the content of CN. The mixing of ECN and the solution of CMCN gave viscous solution and became gel. Fig. 4.2(g) shows the similar FTIR spectrum to that of CMCNB gel except the intensity of amino group as identified by using the curve fitting analysis [32].

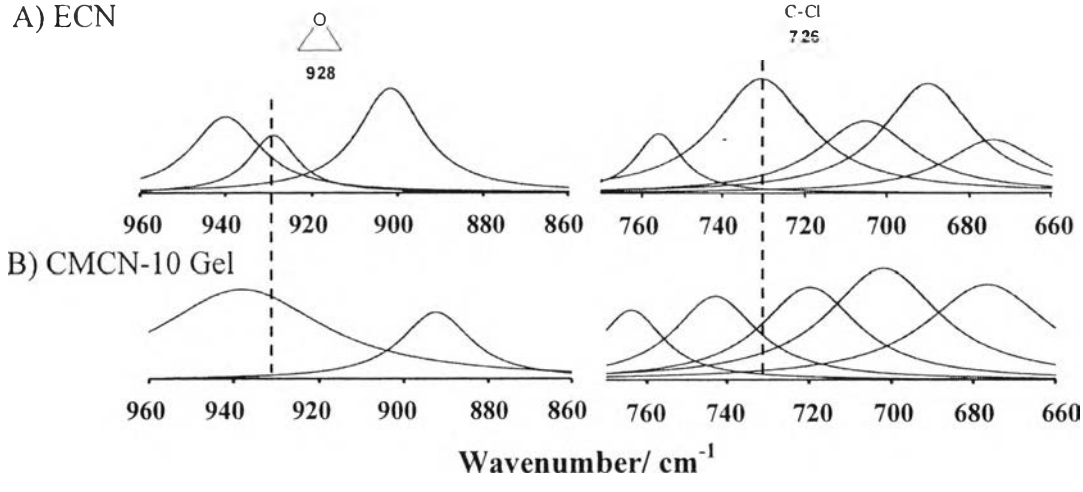

Fig. 4.3 Curve fitting FTIR spectra of (A) ECN and (B) CMCNE-10 gel at 960-860 cm^{-1}, and 760-660 cm^{-1}.

As shown in Fig. 4.3, the disappearances of oxirane ring at 928 cm^{-1} and C-Cl at 726 cm^{-1} are confirmed Based on this result, the mechanism of gel formation of CMCNE gel can be proposed as Scheme 4.5. ^{1}H-NMR is also able to confirm chemical structure of CN and percent deacetylation (% DA) of CN. From ^{1}H-NMR of CN, it can calculate average percent deacetylation by using equation (9) [33].

$$DA\ (\%) = [(ICH3/3)/(IH2\text{-}H6)/6)] \times 100 \qquad (9)$$

Percent DA of CN was found to be 7 (Fig. 4.4(a)). ^{1}H-NMR was applied to determine the degree of substitution CN and CMCN. Fig. 4.4(b) shows the substitution of carboxymethyl groups on 6-O-, 3-O, and 2-N- which can be quantified according to the equations as follows[34].

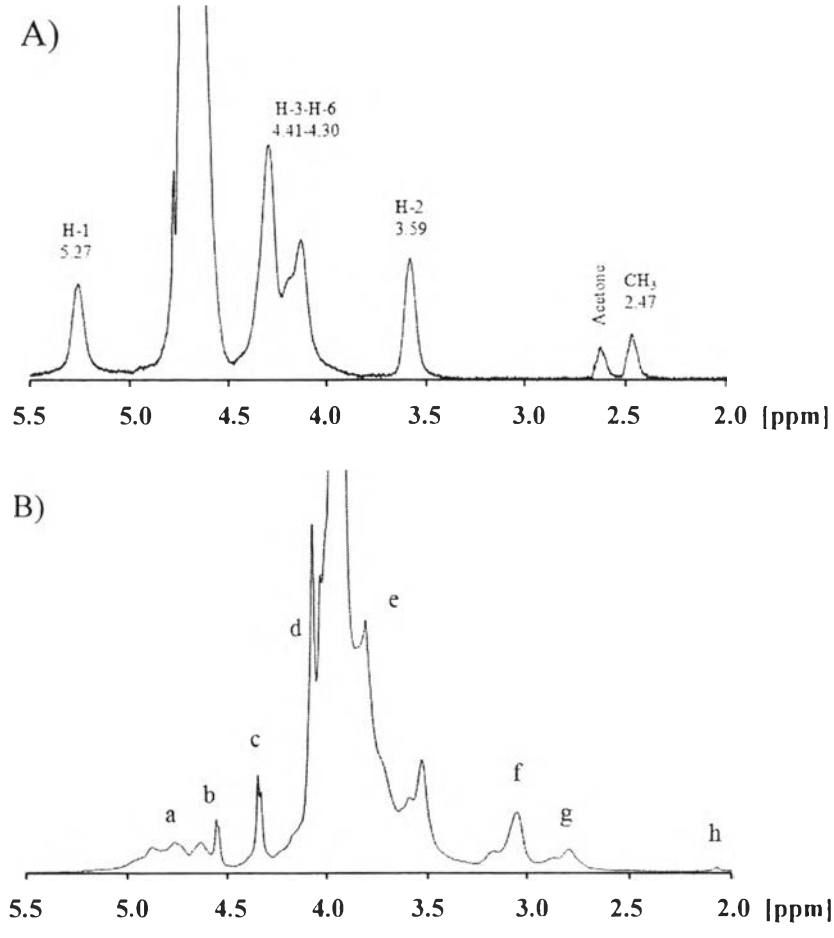

Fig. 4.4 ^{1}H-NMR spectra of (A) CN in 2%CD_3COOD/D_2O at 65 °C and (B) CMCN in D_2O at 25 °C (500 MHz; 300 K). (a) (H1 of GlcN), (b) (H1 of GlcNAc), (c) (H3 of O-CH_2COOH), (d) (H6 and H3 of O-CH_2COOH), (e) (H3-6 of pyranose ring), (f) (H2 of N-CH_2COOH), (g) (H2 of GlcN unit in chitosan), (h) (H2 GlcN unit in chitin).

$$F = f_6 + f_3 + f_N \qquad (10)$$

$$f_6 = 0.5(I_d - I_c)/(I_b + I_g) \qquad (11)$$

$$f_3 = 0.5(I_c)/(I_b + I_g) \qquad (12)$$

$$f_N = 0.5(I_f)/(I_b + I_g) \qquad (13)$$

Herein, F is the total fraction of carboxymethylation, f_6; f_3 and f_N are the fractions of carboxymethylation at the position 6-O-, 3-O- and 2-N-, respectively. The maximum of F is 3.0 for CMCN in this condition. It equals to 1.88 (f_6 = 0.99; f_3 = 0.36, and f_N = 0.52).

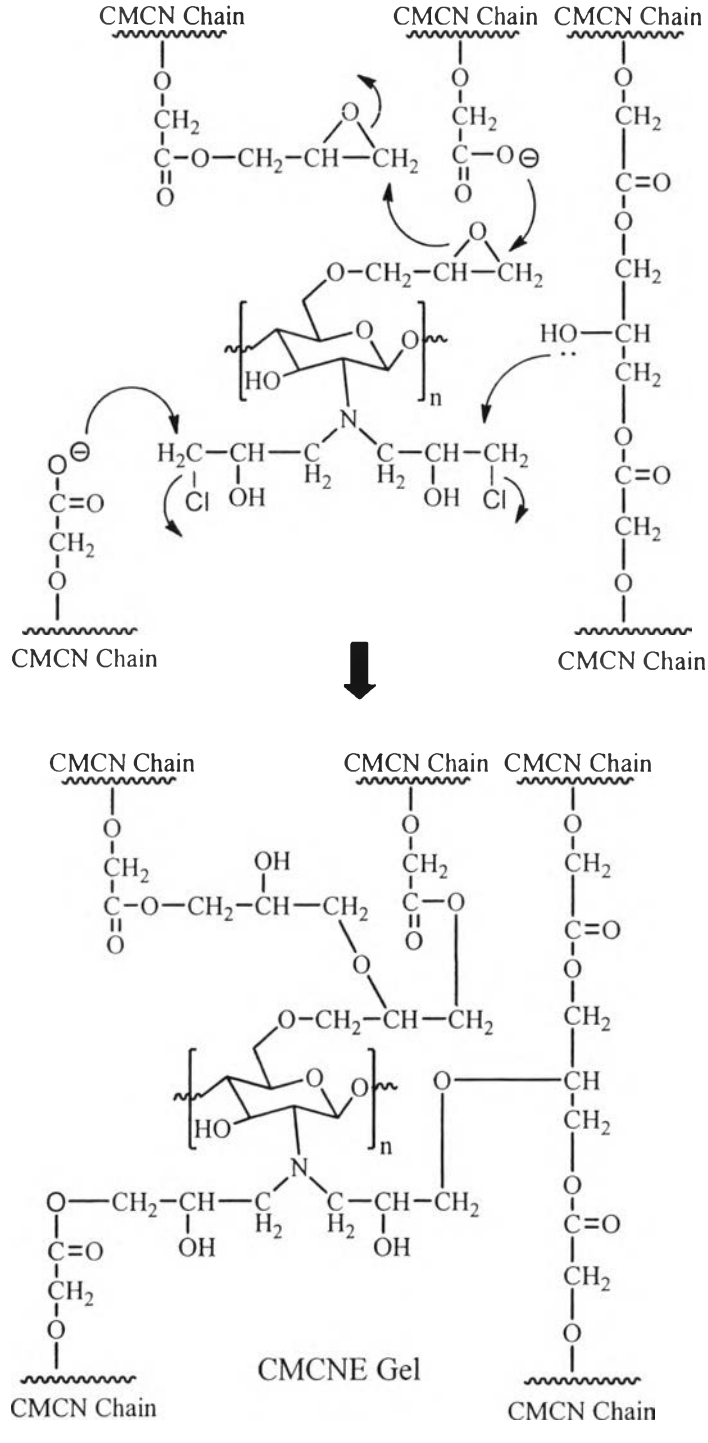

Scheme 4.5 Expected mechanism of gel formation of CMCNE gel

4.4.2 Solubility of CMCN

The solubility of CMCN was examined in a wide range of pH [35]. The pH of the solution was adjusted with 1.0 mol/L HCl and NaOH. Table 4.1 shows a good

solubility of CMCN in the pH range of 6.0 to 14.0 which is a good condition when we consider the pH range of human body system (6.8 to 7.4).

4.4.3 Gel Formation

Gel formation was studied under various amounts of CMCN and EPC from room temperature to 60 °C for 3 h. The test tube inverting method is used to determine gel formation [36]. As shown in Table 4.2, the concentration was suitable for forming gel is 10 to 20 % (w/v) which obtained CMCN-10 to CMC-20 gel and the amount of EPC is 0.2 ml. This condition gives the gel within 45 minutes and gel strength is good enough to study other experiments.

Table 4.1 Water solubility of CMCN in different concentrations and pHs

Type of Solution	pH								
	1	2	4	6	7	8	10	12	14
CMCN-0.5									
CMCN-1									
CMCN-2									
CMCN-3									
CMCN-4									
CMCN-5									
CMCN-10									
CMCN-15									
CMCN-20									

Insoluble Soluble

Table 4.2. Gel formation under various concentrations of CMCN and amount of EPC

EPC (mmol)	Type of Gel						
	CMCN-2	CMCN-4	CMCN-6	CMCN-8	CMCN-10	CMCN-15	CMCN-20
0.0							
0.6							
1.2							
2.5							
3.8							
5.1							
6.3							

No Gelation Gelation

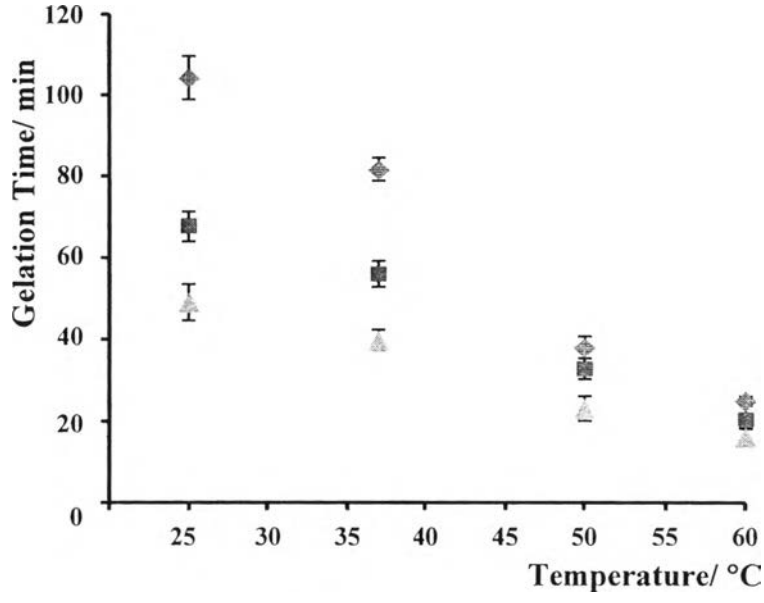

Fig. 4.5 Gelation time of (♦) CMCN-10, (■) CMCN-15, (▲) CMCN-20 gel from test tube inverting method.

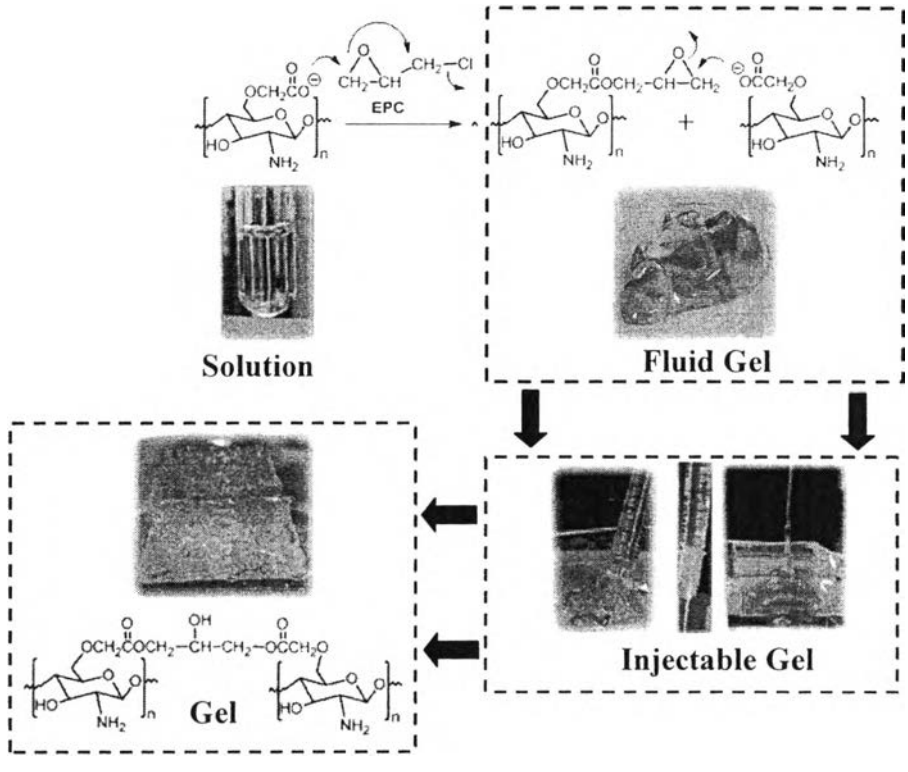

Fig. 4.6 Injectable gel for bone glue material.

For CMCNB and CMCNE gel, it was applied in same condition of CMCN gel to find gelation time and gelation temperature. However, both CMCNB and

CMCNE gel showed same results with CMCN gel, so in the gel formation, gelation time, and gelation temperature, our group showed only CMCN-gel. The gelation time also shows in Fig. 4.5. The results indicate that gelation time reduces when the concentration of CMCN was increased. When CN and ECN were added in CMCN-10 solution, the gelation was confirmed at same condition. All gel solutions were viscous and were injectable through syringe to mold and before forming form gel at room temperature as shown in Fig.4.6.

4.4 Swelling Characteristics

Percent swelling of three types of gels is shown in Fig. 4.7. As compared to CMCN-10 gel, CMCNB gel shows the higher swelling rate and higher percent swelling (Fig. 4.7(a)) when CN was added into CMCN from 2% to 20% (CMCNB-2 toCMCNB-20). This might be due to CN reinforces gel strength with hydrogen bond and promotes water absorption. However, once the amount of CN is more than 40%, the gel performs low swelling rate and percent swelling. It should be noted that a high amount of CN obstructs the chain extension and water absorption. As compared with CMCNE gel (Fig. 4.7(b)), all CMCNE gels shows slow swelling rate but more continuous rate. Thus, CMCNE gels eventually show higher percent of swelling more than CMCNB gel, even the amount of ECN equal to 60 % in hydrogel. This might be due to the fact that ECN can form covalent bond with gel matrices. From this reason, CMCNE gels perform higher percent of swelling and trend to show higher gel strength. Mechanism of water uptake and EWC are shown in the table 4.3. EWC of CMCNB gel trends to reduce when increasing amount of CN, but in case of CMCNE gel it shows increasing of EWC until 20 percents of ECN. However, when the amount of ECN is more than 40 percents, it shows reducing of EWC from effect of solid scaffold in gel. The swelling exponent (n) for the hydrogel is calculated by using Eq. (4). All gels show the same mechanism of water uptake as non-Fickian.

4.5 Network Parameters

M_c was calculated by using Eq. (5), ϕ was calculated by using Eq. (6), χ parameter was examined by using Eq. (7), and V_e was determined by using Eq. (8),

these results display in table 4. The properties of injectable gel are important in the estimate of potential as a bone glue material. The most basic parameters are polymer volume fraction, ϕ, average molecular weight between crosslinks, M_c, and the crosslink density, V_e, in equilibrium swollen state. The volume fraction of polymer, ϕ, explains the amount of liquid which can be absorbed into hydrogels and is interpreted as a ratio of the polymer volume to the swollen gel volume [37].

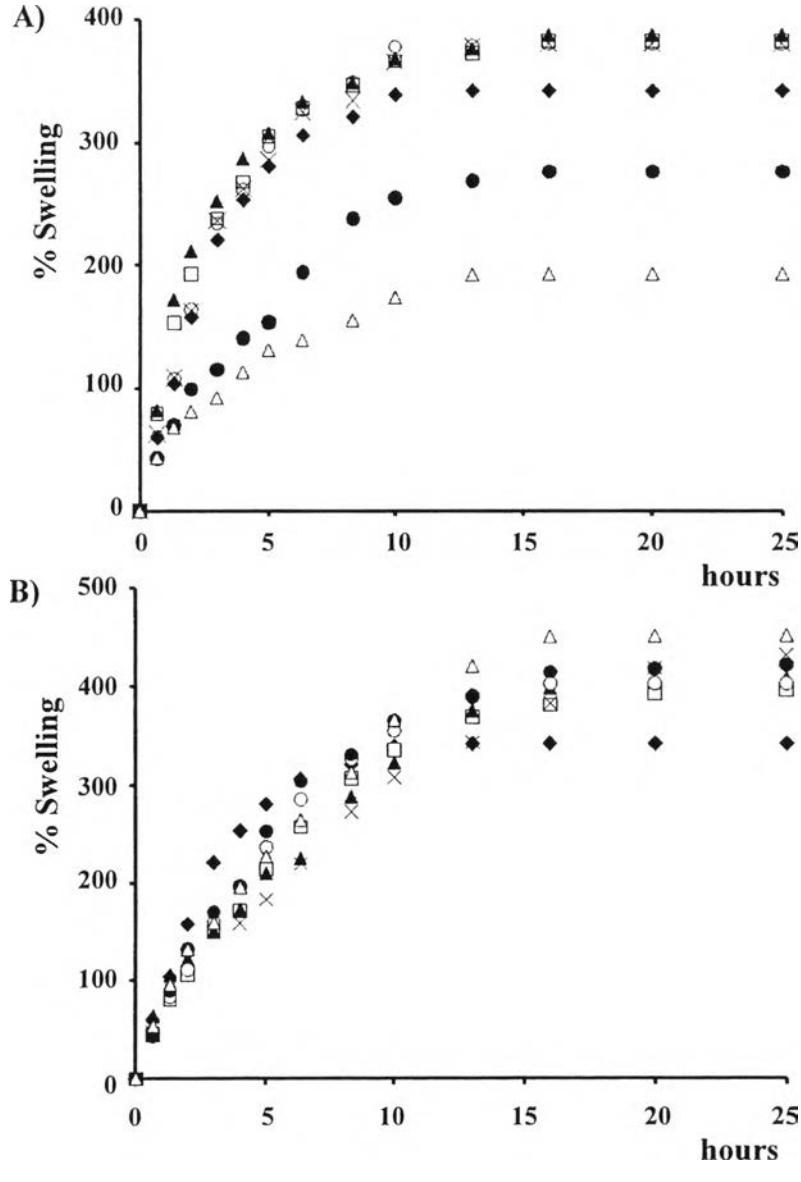

Fig. 4.7 Percent swelling of A) (♦) CMCN-10 gel comparing to CMCNB- (□) 2, (▲)5, (×)10, (○)20, (•)40, and (Δ)60 gel, and B) (♦) CMCN gel comparing to CMCNE(□)2%, (▲)5%, (×)10%, (○)20%, (•)40% and (Δ)60%) gel, (n = 5, SD ≤ 10).

Table 4.3 Equilibrium water content (EWC) and diffusion characteristics

Gel	EWC	n	Mechanism
CMCN-10	191.6	0.60	non-Fickian
CMCNB-2	191.3	0.64	non-Fickian
CMCNB-5	174.8	0.67	non-Fickian
CMCNB-10	134.5	0.70	non-Fickian
CMCNB-20	121.6	0.64	non-Fickian
CMCNB-40	72.3	0.62	non-Fickian
CMCNB-60	35.7	0.52	non-Fickian
CMCNE-2	259.1	0.73	non-Fickian
CMCNE-5	296.7	0.58	non-Fickian
CMCNE-10	294.0	0.68	non-Fickian
CMCNE-20	232.7	0.69	non-Fickian
CMCNE-40	165.7	0.67	non-Fickian
CMCNE-60	129.9	0.69	non-Fickian

In this study, ϕ is nearly alike except when the amount of CN more than 40% (CMCNB-40). It shows increasing of ϕ. From this result, it might be due to high amount of CN is able to extend polymer volume in CMCNB gel. However, in case of CMCNE gel that is expected can form covalent bond with gel matrices, their show a nearly constant volume fraction of polymer. Even though, the percent of ECN equals to 60. For the polymer–water interaction parameter (χ), we can assume that it is alike except 60 percents of CN. This interaction might be increased from CN.

In case of M_c, These are chains between two consecutive junctions. These junctions may be chemical crosslinks, physical entanglements, or even polymer complexes [20]. It illustrates when we add CN to produce CMCNB gel. Our group observes that M_c trend to decrease, and the pore density in the injectable gel increases. For CMCNE gel, it shows higher Mc more than CMCN gel even though 60 percents of ECN. From this result, it means that ECN can form covalent bond with gel matrices so it displays high M_c. However, when the amount of ECN increased, the trend shows to decrease of Mc similar to CMCNB gel. It is well-known that M_c values increase, whereas the effective crosslink densities (V_e) of polymer networks

decrease. For CMCNB gel, it illustrates a slight increasing of V_e except 60 percents of CN (CMCNB-60). For CMCNE gel, it shows reducing of V_e and then, it shows a slight increasing of V_e.

Table 4.4 Network parameters of injectable gel

Gel	ϕ	χ	M_c ($\times 10^{-3}$ g/ mol)	$V_e \times 10^{-19}$
CMCN-10	0.19	0.56	31.3	2.35
CMCNB-2	0.19	0.56	30.0	2.38
CMCNB-5	0.19	0.56	28.8	2.41
CMCNB-10	0.20	0.57	25.8	2.53
CMCNB-20	0.20	0.57	25.9	2.51
CMCNB-40	0.25	0.58	9.8	6.62
CMCNB-60	0.33	0.61	3.3	19.1
CMCNE-2	0.15	0.55	86.8	0.97
CMCNE-5	0.17	0.56	70.1	1.06
CMCNE-10	0.16	0.55	62.2	1.17
CMCNE-20	0.16	0.55	64.1	1.21
CMCNE-40	0.16	0.55	60.1	1.25
CMCNE-60	0.16	0.55	56.2	1.22

4.6 Morphology Observation

The morphologies of CW and CN were investigated by transmission electron microscopy (TEM). CW shows fibers in nanoscale (Fig. 4.1(a)). After deacetylation CW has developed itself to three dimensional nanofiber networks or so-called CN (Fig. 4.1(b)) [15]. It shows an increase in surface area, pore volume, pore size. When we modified new functional group on surface of CN with heterogeneous reaction to obtain ECN, we can prove that the reaction can maintain former morphology of CN via TEM (Fig. 4.8(b)). The morphologies of CMCN-10 gel, CMCNB-10 gel, and CMCNE-10 gel were also observed by optical microscope and scanning electron microscope. As shown in optical microscope (Fig. 4.9), as compared to CMCN-10 gel, CMCNB-10 gel and CMCNE-10 gel are the ones

containing nanofiber network to reinforce gel strength and to promote cell proliferation.

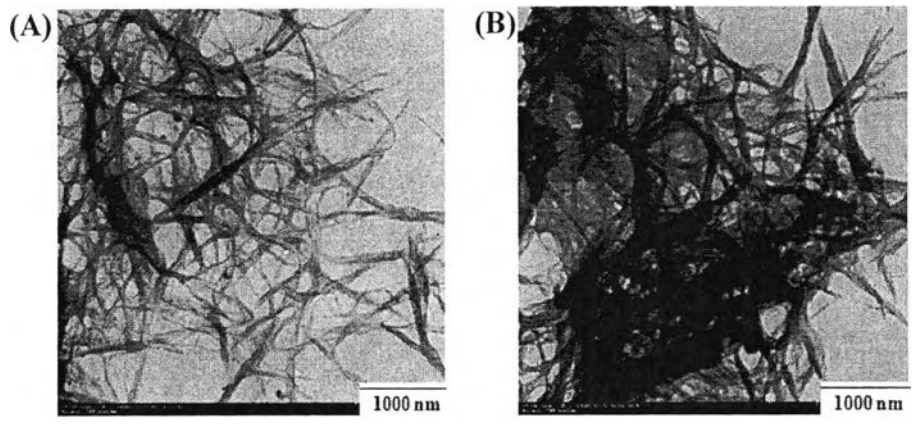

Fig. 4.8 TEM micrographs of (A) CN, and (B) ECN.

However, CMCNE-10 gel shows good distribution of nanofiber network more than CMCNB-10 gel. This might be due to 10% ECN formed covalent bonds within matrices of gel. The morphologies of CMCN-10 gel, CMCNB-10 gel, and CMCNE-10 gel gel are shown by SEM. It is important to note that compatibility of nanofiber network between chitosan nanoscaffold and chitosan matrices can be confirmed. From these morphologies, three types of gel are promising novel injectable gel.

4.7 Rheological Analysis

The plot of storage modulus (G′) and loss modulus (G″) is shown in Fig. 4.10. Three types of gel demonstrate the long linear viscoelastic (LVE) range (around 80 % strains) because they were formed by covalent bond. The storage modulus can be used to represent the strength of gel. As added nanofiber network (CN or ECN) into injectable gel, both CMCB-10 and CMCNE-10 gel illustrate higher G′ than that of CMCN-10 gel around 2 times. This might be due to nanofiber network (CN or ECN) promotes gel strength of injectable gel. In the case of CMCNE-10 gel, it shows a little bit higher G′ than that of CMCB-10 gel.

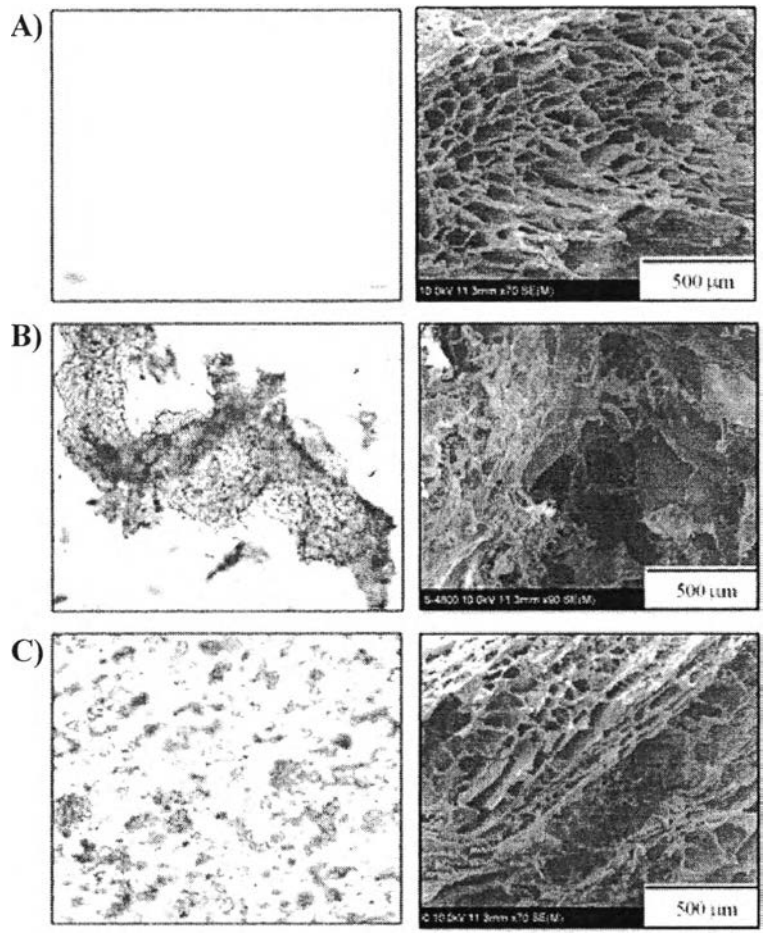

Fig. 4.9 Optical micrographs (left) and SEM micrograph (right) of (A) CMCN-10 gel, (B) CMCNB-10 gel, and (C) CMCNE-10 gel.

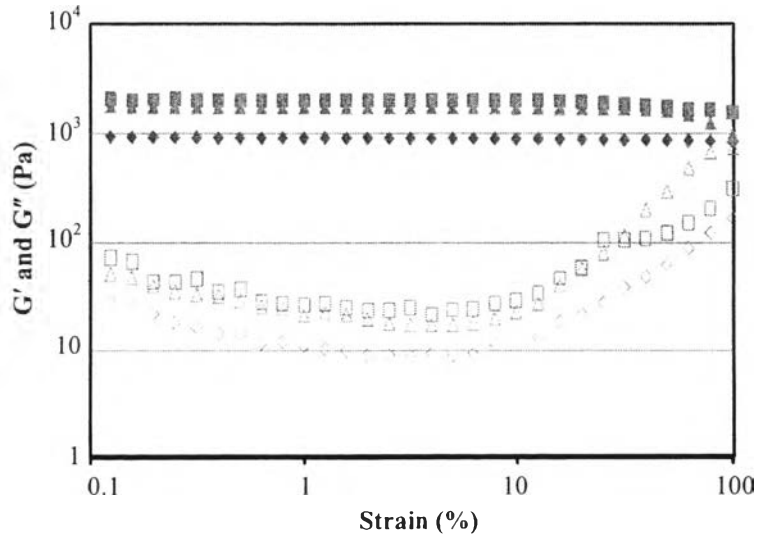

Fig. 4.10 Storage modulus (G′) of CMCN-10 (♦), CMCNB-10 (▲) and CMCNE-10 (■) gel and loss modulus (G″) of CMCN-10 (◊), CMCNB-10 (△) and CMCNE-10 (□) gel.

Because of nanofiber formed not only primary force (covalent bond) but also secondary force (hydrogen bond) with gel matrices.

4.8 Mineralization with Hydroxyapatite on Injectable Gel

The attractive points of injectable gel are not only for directly injectable to broken bone, but also for inducing to accumulate hydroxyapatite for broken bone. Previously, Tachaboonyakiat et al. reported that hydroxyapatite (HA) was formed by alternate soaking with calcium chloride and sodium hydrogen phosphate. The HA formation was expected as the following stoichiometric relationship [21]

$$10CaCl_2 + 6Na_2HPO_4 + 2H_2O \longrightarrow Ca_{10}(PO_4)_6(OH)_2 + 12NaCl + 8HCl$$

We found that injectable gel showed a constant shape after soaking and CMCN-10, CMCNB-10, and CMCNE-10 gel were able to cooperate with HA (Fig. 4.11). TGA was used to evaluate the amount of HA in three types of gel. Herein, it was assumed that the percent increasing in ash content of the gel with HA (Fig. 4.12). The HA amounts of the first cycle of CMCN-10, CMCNB-10, and CMCNE-10 gel are increase around 10%, 12% and 19%, respectively.

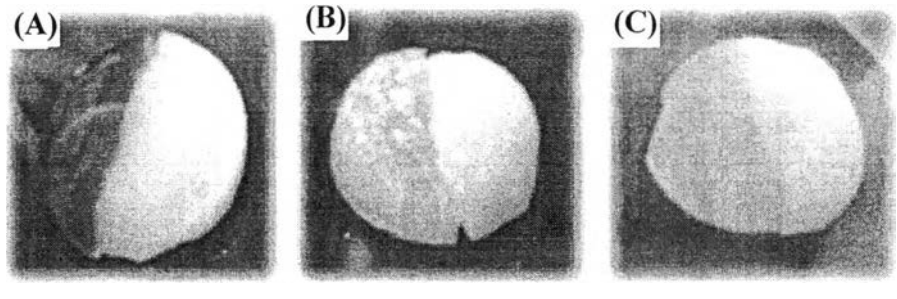

Fig. 4.11 Three types of gels, (A) CMCN-10, (B) CMCNB-10, and (C) CMCNE-10 gel, left hand original gel and right hand gel after mineralization with hydroxyapatite for 3 times.

The HA content after soaking for five times of CMCN-10, CMCNB-10, and CMCNE-10 gel are 60%, 61% and 67%, respectively. After mineralization with HA, All gels show higher hardness than original ones. The reason of high HA content in

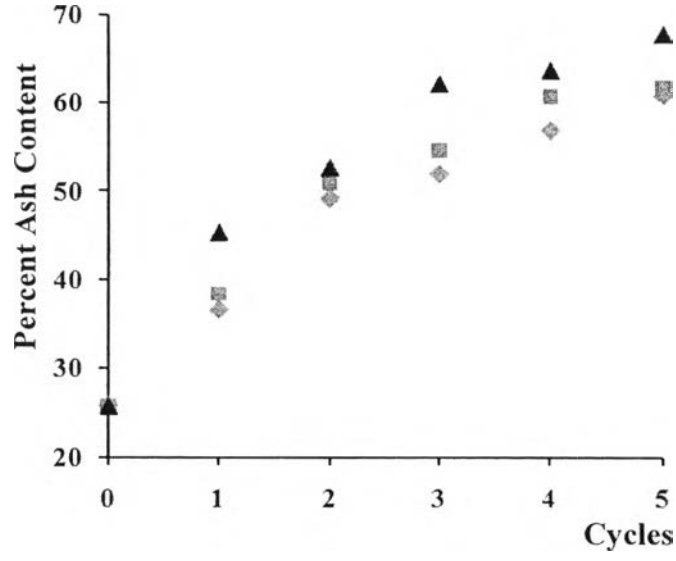

Fig. 4.12 Percent ash content of (♦) CMCN-10, (■) CMCNB-10, and (▲) CMCNE-10 gel by alternate soaking.

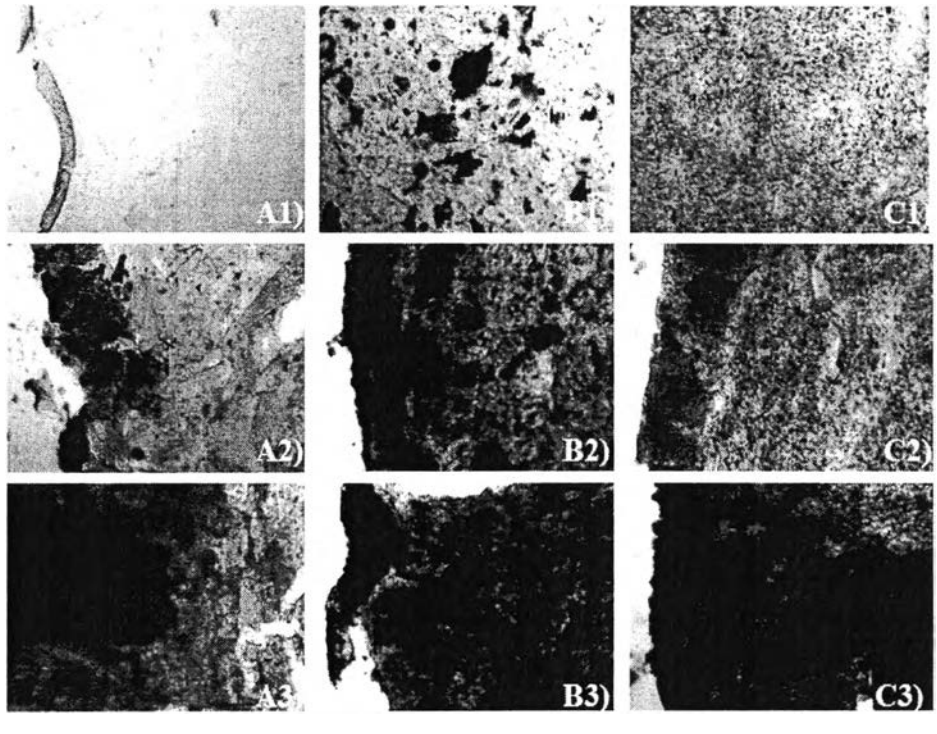

Fig. 4.13 Optical micrographs of HA formation of, (A) CMCN-10 gel, (B) CMCNB-10 gel, and (C) CMCNE-10 gel (number is cycle of soaking).

CST gel, we can consider from Fig 4.13. The first time, HA (black color) chooses to form itself at scaffold of both CS and CST in gel. Next, it forms in the gel matrices

especially at an edge of gel. SEM micrographs show the same result of HA formation with optical microscopy (Fig. 4.14).

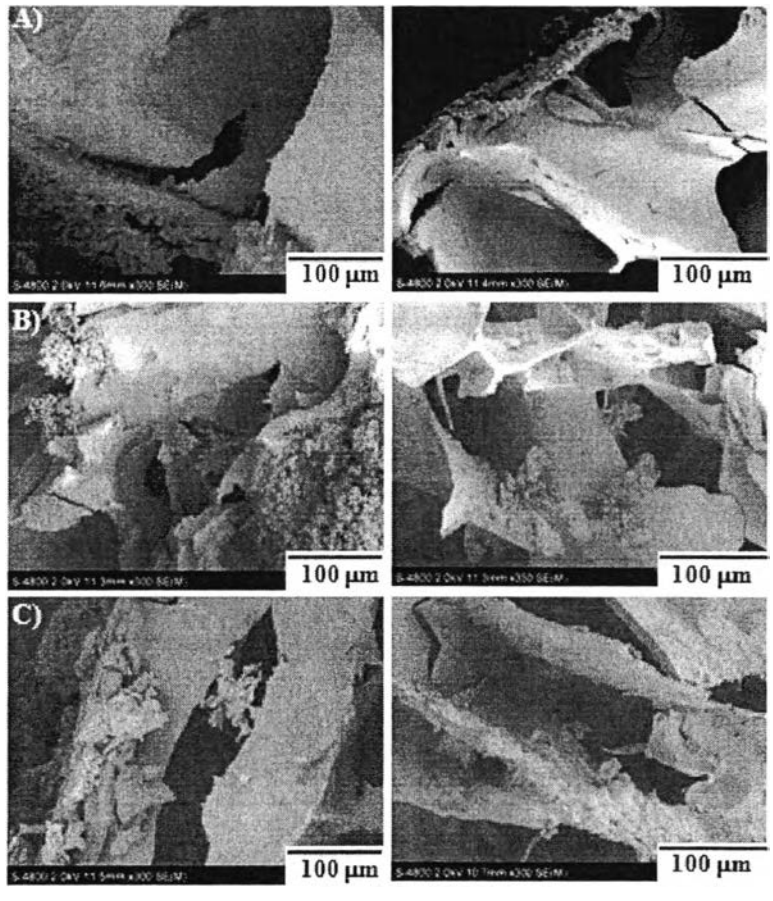

Fig. 4.14 SEM micrographs of HA formation of, A) CMCN-10 gel, (B) CMCNB-10 gel, and (C) CMCNE-10 gel.

4.9 Cell Culture Studies

For cell culture test, we used direct contatc of SaOs-2 cells (one type of cell bone) to determine toxicity of all gels by DNA assay technique.As shown in Fig. 4.15, All gels are non-toxic and trend to induce cell growth. When we compare the number of cell between 6h and 7d, we found that percent cell growth of CMCN-10, CMCB-10, and CMCNE-10 gel is 4.86, 14.02, and 11.10% repectively. From the results, we can confirm the injectable bionanocomposite can enhanc bone cell generation more than only injectable gel. It might be due to three dimensional nanofiber network promoting cell growth by supporting cells attachment.

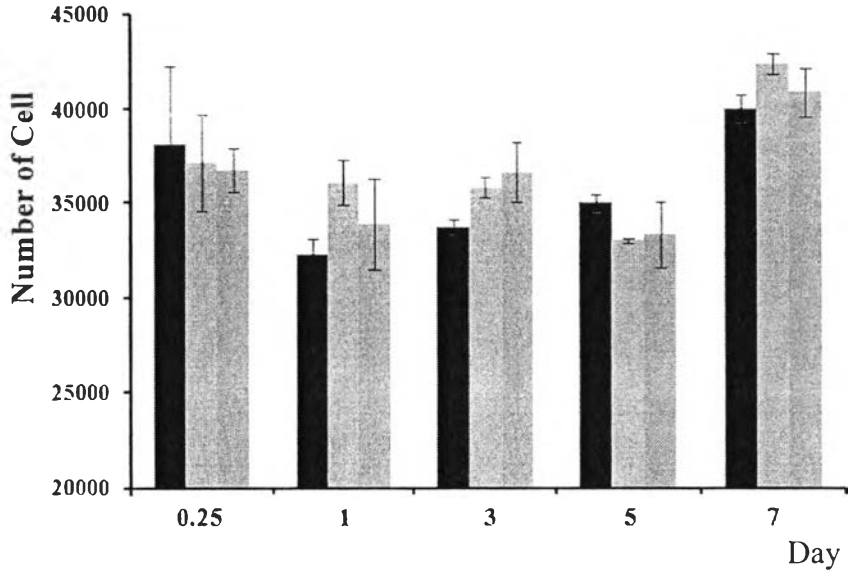

Fig. 4.15 Number of SaOs-2 cells from DNA assays of (■) CMCN-10, (■) CMCNB-10, and (■) CMCNE-10 gel.

4.10 Conclusions

Chitosan nanoscaffold injectable gel for bone glue material can be produced by using chitosan derivative. Chitin flake to modify as CN, ECN, and CMCN. All products can be produced three types of injectable gel via ring opening with EPC to form crosslinked under body temperature without using organic solvent. Both CMCNB-10 and CMCNE-10 gel as bionanocomposite performed many good properties more than CMCN-10 gel. From the properties of the injectable gel, it has a potential bone glue material for bone regeneration.

4.11 References

[1] Kaufman, J.J., and Chiabrera, A.E. (1997) U.S. Patent. 5, 651-363.

[2] Guillen, G.P., and Madroñero, A.C. (1985) J. Biomed. Eng. 7, 157-160.

[3] Hulstyn, M., Fadale, P.D., Abate, J., and Walsh, W.R. (1993) Arthroscopy. 9, 417-424.

[4] Jager, T., Journeau, P., Dautel, G., Barbary, S., Haumont, T., and Lascombes, P. (2010) Orthop. Traumatol. Surg. Res. 96, 340-347.

[5] Zhang, R., and Ma, P.X. (1999) J. Biomed. Mater. Res. 45, 285–293.

[6] Ishaug, S.L., Crane, G.M., Miller, M.J., Yasko, A.W., Yaszemski, M.J., and Mikos, A.G. (1997) J. Biomed. Mater. Res. 36, 17–28.

[7] Ma, PX., Zhang, R., and Xiao, G. (2001) J. Biomed. Mater. Res. 54, 284–293.

[8] Chenite, A., Chaput, C., Wang, D., Combes, C., Buschmann, M.D., Hoemann, C.D., Leroux, J.C., Atkinson, B.L., Binette, F. and Selmani, A. (2000) Biomaterials. 21, 2155-2161.

[9] Rinaudo, M. (2006) Prog. Polym. Sci. 31, 603-632.

[10] Yamamoto, H., and Amaike, M. (1997) Macro-molecules. 30, 3936-3937.

[11] Freesia, L.H., and Warren, H.E. (1972) Biochim. Biophys. Acta. 273, 157-164.

[12] Seiichi, T., and Hiroshi, T. (2001) Biomacro-molecules. 2, 417-421.

[13] Manjubala, I., Scheler, S., Jörf, B., and Klaus, D. (2006) Acta Biomate. 2, 75-84.

[14] Shi, Z.L., Neoh, K.G., Kang, E.T., Poh, C.K., and Wang, W. (2009) Biomacromolecules. 10, 1603-1611.

[15] Phongying, S., Aiba, S. and Chirachanchai, S. (2007) Polymer. 48, 393–400.

[16] Phongying, S., Aiba, S., and Chirachanchai, S. (2007) Polymer. 48, 393-400.

[17] Zhou, J., Lee, M.J., Jiang, P., Henderson, S. and Lee, D.G. (2010) J. Thorac. Cardiov. Surg. 140, 801-806.

[18] Liping, S., Yumin, D., Lihong, F., Xiao, C., and Jianhong, Y. (2006) Polymer. 47, 1796-1804.

[19] Chen, L., Tian, Z., Du Y. (2004) Biomaterials. 25, 3725-3732.

[20] Nair K.G., and Dufresne A. (2003) Biomacro-molecules. 4, 666.

[21] Lingyun, C., Yumin, D., Zhigang, T., and Liping, S. (2005) J. Polym. Sci. 43, 296-305.

[22] Wang, J., and Wu,W. (2005) Eur. Polym. J. 41, 1143–1151.

[23] Thakur, R.R.S., Woolfson, A.D., and Donnelly, R.F. (2010) J. Pharm. Pharmacol. 62, 829–837.

[24] Sunil, K.B., Surinderpal, S. (2006) React. Funct. Polym. 66, 431-440.

[25] Paul, J.F., and John, R.J. (1943) J. Chem. Phys. 11, 512–517.

[26] Jordan, R.N. (1983) Fuel. 62, 113-116.

[27] Martin, J.G., Thakur, R.S., David, A. W., and Ryan F. D. (2010) Int. J. Pharm. 406, 91–98.

[28] Tuncer, C., Simin, K., and GöKhan, D. (2006) J. Appl. Polym. Sci. 101, 1756–1762.

[29] Sunil, K.B., and Surinderpal, S. (2006) React. Funct. Polym. 66, 431–440.

[30] Ramazani-Harandi, M.J., Zohuriaan-Mehr M.J., Yousefi, A.A., Ershad Langroudi, A., and Kabiri, K. (2006) Polym. Test. 25, 470-474.

[31] Tachaboonyakiat W, Serizawa T, and Akashi M. (2001) Polym. J. 33, 177-181.

[32] Sandler, S.R., Karo, W., Bonesteel, J., and Pearce, E.M. (1998) *Polymer synthesis and characterization.* pp 61. New York, Academic Press.

[33] Mohammad, R.K. (2010) Carbohydr. Polym. 79, 801-810.

[34] Chena, X.G., and Park, H.J. (2003) Carbohydr. Polym. 53, 355-359.

[35] Zhang, C., Ping, Q., Zhang, H., and Shen, J. (2003) Eur. Polym. J. 39, 1629–1634.

[36] Narayan, B., Hassna, R. R., Jonathan, G., Frederick , A. M., and Miqin, Z. (2005) J. Controlled Release. 103, 609–624.

[37] Tuncer, C., Recai, I. (2004) J. Appl. Polym. Sci. 91, 2168–2175.